Atmos. Chem. Phys. Discuss., 13, 16337–16366, 2013
www.atmos-chem-phys-discuss.net/13/16337/2013/
doi:10.5194/acpd-13-16337-2013

Atmospheric Chemistry and Physics Discussions

Tropospheric carbon monoxide variability from AIRS and IASI under clear and cloudy conditions

J. Warner[1], F. Carminati[1,2,4], Z. Wei[1], W. Lahoz[2,5], and J.-L. Attié[2,3,4]

[1]Department of Atmospheric and Oceanic Science, University of Maryland, 3433 Computer and Space Sciences Bldg, College Park, MD 20742, USA
[2]CNRM-GAME, Météo-France and CNRS, UMR3589, Toulouse, France
[3]Laboratoire d'Aérologie, CNRS, UMR5560, Toulouse, France
[4]Université de Toulouse, Toulouse, France
[5]Norwegian Institute of Air Research, Instituttveien 18, Kjeller 2027, Norway

Received: 6 May 2013 – Accepted: 29 May 2013 – Published: 18 June 2013

Correspondence to: J. Warner (juying@atmos.umd.edu)

Published by Copernicus Publications on behalf of the European Geosciences Union.

Abstract

We study the Carbon Monoxide (CO) variability in the last decade measured by NASA's Atmospheric InfraRed Sounder (AIRS) on the Earth Observing Systems (EOS)/Aqua satellite and Europe's Infrared Atmospheric Sounder Interferometer (IASI) on MetOp platform. The focus of this study is to analyze CO variability and short-term trends separately for background CO and new emissions based on a new statistical approach. The AIRS Level 2 (L2) retrieval algorithm, as well as the IASI products from NOAA, utilizes cloud clearing to treat cloud contaminations in the signals; and this increases the data coverage significantly to a yield of more than 50 % of the total measurements (Susskind et al., 2003). We first study if the cloud clearing affects CO retrievals and the subsequent trend studies by using the collocated Moderate Resolution Imaging Spectroradiometer (MODIS) (Ackerman et al., 1998) cloud mask to identify AIRS clear sky scenes. We then separate AIRS CO data into clear and cloud-cleared scenes and into background and new emissions, respectively. Furthermore, we carry out a similar study for the IASI CO and discuss the consistency with AIRS. We validate the CO variability of the emissions developed from AIRS against other emission inventory databases (i.e., Global Fire Emissions Database – GFED3 and the MACC/CityZEN UE – MACCity) and calculate that the correlation coefficients between the AIRS CO emissions and the emission inventory databases are 0.726 for the Northern Hemisphere (NH) and 0.915 for the Southern Hemisphere (SH).

1 Introduction

Global long-term measurements of tropospheric Carbon Monoxide (CO) from space borne instruments have been possible since year 2000 with the launch of the Measurement Of Pollution In The Troposphere (MOPITT) (Drummond, 1989) on the Earth Observing Systems (EOS) Terra satellite, followed by the Atmospheric InfraRed Sounder (AIRS) on Aqua (Aumman et al., 2003), the Tropospheric Emission Spectrometer (TES)

ACPD
13, 16337–16366, 2013

on Aura (Beer, 2006), and the Infrared Atmospheric Sounder Interferometer (IASI) on the European MetOp platform (Clerbaux et al., 2010). These measurements have advanced our understanding in many areas of science such as air quality and transport studies (Heald et al., 2003; Lin et al., 2012); field campaign support and validation (Fisher et al., 2010; Emmons et al., 2004, 2007; Warner et al., 2007); model chemistry, transport, and data assimilation studies (Kim et al., 2013; Lamarque et al., 2004; Arellano et al., 2007; Pradier et al., 2005) that aim to improve the capability of air quality forecasts.

There has been attention recently on the CO trend using satellite measurements, especially considering that the lifetime of MOPITT and AIRS has exceeded 10 yr (Worden et al., 2013; He et al., 2013). These studies have found a decreasing trend in a number of regions that are possibly due to the increased air quality standards and economic slowdown. This manuscript re-examines the short-term CO trends from AIRS and IASI with a focus on the discussion of the background CO and new emissions. Separating CO new emissions from the background is of interest in that the background CO variability can be used to validate modeled CO climatology, which in turn benefits air quality forecasts. Inventory studies based on CO measurements largely rely on the use of inverse modeling and top-down estimates (Pfister et al., 2005; Arellano et al., 2006; Kopacz et al., 2010). The capability to separate the new emissions from the background CO may also lead to an automated real-time detection system for fire emissions. Although near-real time fire detection from the Moderate Resolution Imaging Spectroradiometer (MODIS) products based on the surface biomass properties is available (Justice et al., 2002), the CO based fire detection has not been used hitherto.

AIRS provides twice daily and near global coverage of tropospheric CO for a period from 2002 through the lifetime of AIRS, and the consistent CO climate record will continue with IASI instruments for the current and planned missions of 15 yr started in late 2006. IASI is a Fourier transform spectrometer onboard the meteorological platform MetOp-A, launched at the end of 2006 by the European Space Agency. IASI has similar temporal and spatial coverage as AIRS and both are hyperspectral thermal

ACPD
13, 16337–16366, 2013

sensors. This study uses the operational AIRS CO products that are based on AIRS science team physical algorithms and distributed by the NASA GSFC's Earth Sciences (GES) Distributed Active Archive Center (DAAC). The IASI CO products, from NOAA, used in this study are retrieved very similarly to AIRS CO to minimize biases between the two datasets.

Satellite measurements using the thermal spectral regions are affected by the presence of clouds and, therefore, it is necessary to remove the effects of clouds before retrieving many geophysical properties. Techniques to remove cloud contamination include the identification and removal of the entire pixel that contains clouds, referred as cloud detection. An example of using cloud detection for the MOPITT level-2 (L2) algorithm is given by Warner et al. (2001). Another approach is to reconstruct clear column radiances that would have been there if there were no clouds, referred to as cloud clearing. Many earlier studies (Smith 1968; Chahine, 1974; McMillin et al., 1982; Susskind et al., 1998) have built the foundation for the cloud clearing technique that was later used in a number of satellite instrument algorithms.

The AIRS L2 retrieval algorithm utilizes cloud clearing to remove cloud contamination in the radiances and this helps to increase the L2 data coverage significantly to a yield of 50–70 % of the total measurements. AIRS' cloud clearing uses 9 neighboring pixels with different cloud fractions to solve for clear radiances, which also requires the microwave sounder Advanced Microwave Sounding Unit (AMSU) data (Susskind et al., 2003). Cloud clearing utilizes the contrast in the cloud fraction between neighboring pixels and can recover non-uniform cloudy pixels with up to 80 % of cloud cover. Sounding is performed on a 45 km field of regard (FOR), which is defined by the size of the AMSU footprints. It is important to understand the effects of the cloud clearing on the overall quality of the retrievals. To select AIRS clear pixels, we use the collocated MODIS cloud mask (Ackerman et al., 1998), which applies a number of thresholds from 14 different spectral channels in both visible and thermal regions to identify clouds in a $1 \times 1\,km^2$ field of view (FOV).

ACPD
13, 16337–16366, 2013

We first describe, in Sect. 2, the method to collocate AIRS single-view pixels with the Aqua MODIS cloud mask to identify AIRS clear pixels. We then analyze AIRS CO variability using clear sky pixels identified in the previous section and the cloud-cleared pixels from the L2 products in Sect. 3. In Sect. 4, we introduce a statistical method to separate CO emissions from the background concentrations in AIRS data and compare the results with known CO emission inventories. To demonstrate the potential of this study we show similar approaches using IASI CO, in Sect. 5, and provide detailed comparisons between the two datasets, before summarizing this study in Sect. 6.

2 Identifying AIRS clear-sky coverage

To select AIRS clear sky pixels, we use the MODIS cloud masks (MYD35_L2) (ftp://ladsftp.nascom.nasa.gov/allData/5/MYD35_L2/) taking advantage of the fact that MODIS is on the same satellite Aqua platform as AIRS. An example in Fig. 1 illustrates the method we used to collocate AIRS and MODIS pixels. We first select granules that coincide in time from the two datasets, and then match one center pixel of a granule from each sensor using geo-location information. A predetermined index system, marked as colored boxes in Fig. 1, is then used to include a certain number of the surrounding MODIS pixels for each AIRS pixel. This index system was developed based on a fixed relationship between the AIRS and MODIS instrument viewing angles, which will not change during the lifetime of the sensors. Note that some MODIS pixels are not included between the rectangular boxes to account for the gaps between AIRS scan lines (see Aumann et al., 2003 on AIRS instrument design).

AIRS single FOVs of ~ 13.5 km at nadir are used to collocate with MODIS $1 \times 1\,\mathrm{km}^2$ pixels. We define an AIRS clear pixel when more than 99 % of MODIS pixels inside are flagged to be clear. AIRS clear coverage defined by the MODIS cloud mask is shown in blue in the Fig. 2 upper panel and it is approximately 10–13 %. AIRS clear coverage is also defined by AIRS measurements, instead of by MODIS, as part of the L2 products. The blue pixels in Fig. 2 lower panel show AIRS L2 clear sky cases (CloudFraction = 0)

ACPD
13, 16337–16366, 2013

to be ∼ 22 %, which tends to overestimate the amount of clear coverage compared to the upper panel using the MODIS cloud mask. AIRS L2 cloud fraction products can be compared to those defined by the MODIS cloud mask only under absolute clear sky or completely overcast conditions because the MODIS sub-pixel cloudiness is unknown.

The low clear sky coverage shown as blue pixels in Fig. 2 confirms the needs for cloud clearing in the case of AIRS. This is not only because the clear sky coverage is otherwise only approximately 10 %, but also a large portion of the clear sky coverage is over less populated regions such as at the poles and over the deserts. Thus, if only clear sky measurements were used, the available data over populated regions, where the routine monitoring is essential, would have been significantly fewer than 10 %. This would not have been sufficient to provide daily products for monitoring purposes.

3 AIRS CO variability for clear sky and cloud-cleared scenes

In this section, we discuss the CO differences between AIRS clear sky coverage using the MODIS cloud mask and cloud-cleared datasets to assess the performances of AIRS cloud clearing and identify possible limitations. We analyze the statistics of the AIRS CO distribution and variability using clear pixels and cloud-cleared pixels independently. Note that the CO values for clear pixels are selected from AIRS V5 L2 datasets where the cloud-cleared radiances might have been altered slightly during the cloud clearing process even for clear scenes. Accurate CO values under clear sky conditions should have been the retrieved CO from Level-1 (L1) clear radiances; however, we do not expect large differences between the two datasets. Additionally, the CO data coverage achieved by using cloud clearing is crucial for daily maps, but less critical for three-months mean hemispheric averages that we use in this study.

The monthly mean AIRS V5 CO maps for March to May 2006 are shown in Fig. 3 with the clear daytime cases on the left upper panel, the clear nighttime cases on the left bottom panel, the cloud-cleared daytime cases on the right upper panel, and the cloud-cleared nighttime cases on the right bottom panel. Large areas of the Earth are covered

ACPD
13, 16337–16366, 2013

by clouds throughout the month as shown by the gaps in the left panels demonstrating the need for AIRS cloud-cleared products for monitoring the environment. The elevated CO shows similar emission sources and transport patterns for both the clear sky cases (left panels) and the cloud-cleared cases (right panels). Although the clear sky cases are embedded in the total pixels under discussion, we equate the total pixels as the cloud-cleared cases and believe it is an acceptable approximation due to the large sampling differences between the number of the clear cases and the cloud-cleared cases. In general, the clear sky cases show higher values in the elevated CO regions than the cloud-cleared cases, for both daytime and nighttime. Daytime CO values are generally higher than the nighttime, which is due to the surface thermal contrasts that increase the CO measurement sensitivity and in turn result in higher retrieved CO in the NH (Deeter et al., 2007).

To understand the effect of the cloud clearing on the retrievals, it is important to examine the information content, or the Degrees of Freedom for Signal (DOFS). AIRS operational CO DOFS are calculated in a different formula from that commonly used in the community and described by Rodgers (2000). We computed the DOFS in this study using the Rodgers formula that is generally associated with the optimal estimation (OE) retrievals (Warner et al., 2010), even though the CO values are from AIRS Version-5 (V5) operational products using physical retrievals (Susskind et al., 2003). Figure 4 shows AIRS OE CO DOFS for the months of March to May 2006 for cloud-cleared cases (right panels) versus clear cases (left panels) and for daytime (upper panels) versus nighttime (lower panels). The high DOFS values for the cloud-cleared products range from 0.8 to 1.0, and the DOFS values for the clear sky conditions go up to 1.2. Also note that the DOFS in daytime is higher compared to nighttime due to the difference in surface thermal contrast.

We use Probability Density Functions (PDFs) to study the statistical differences in the CO distributions between using cloud-cleared radiances and using clear scenes. Figure 5 shows PDF plots of AIRS V5 CO VMRs for the NH ocean (upper left), NH land (upper right), SH ocean (lower left), and SH land (lower right), respectively, for the

ACPD
13, 16337–16366, 2013

period of March to May 2006 and for daytime only. Each histogram for clear (solid) or cloud-cleared (dashed) conditions is fitted by two Gaussian functions simultaneously. The left Gaussian fits (blue) in each panel represent a well-mixed background with lower CO values while the right Gaussian fits (red) with higher values represent the CO from new emissions. We define the new emissions as the elevated CO that is seen by satellite instruments, but emitted and transported from the surface. The fitted CO background PDFs (blue curves in Fig. 5) are approximately the same between clear (solid) and cloud-cleared (dotted) cases for both NH and SH oceans (see left panels in Fig. 5). The cloud-cleared PDFs (dotted curves) in the NH show a single mode and a more Gaussian as opposed to the clear cases (solid curves) where a bi-modal feature separating new emissions from the background CO is apparent. The SH land cases show the largest differences between clear and cloud-cleared cases where the cloud clearing masks the otherwise different two populations of background and new emissions (see the lower right panel in Fig. 5). Note, however, this could be partly due to the large sampling differences over the biomass burning regions, where the MODIS cloud mask can misidentify smoke as clouds resulting in very few clear pixels.

Tropospheric CO variability and short-term trends from 2002 through 2011 are summarized, using the modes of the fitted Gaussian functions for each monthly PDF to represent biases, for NH-Land, NH-Ocean, SH-Land, and SH-Ocean, respectively, as shown in Fig. 6. The background values are shown in blue and new emissions in red; while solid curves represent clear sky cases and dashed curves are for cloud-cleared cases. Decreasing trends are shown in most of the years by both clear and cloud-cleared ensembles, which agree with previous studies (Worden et al., 2013; Chevallier et al., 2008). Globally speaking, there is no major bias due to cloud clearing drawing from 9 yr of AIRS CO data records. The clear sky cases, however, show more regular variability for both background and emissions as expected from our previous knowledge of the CO distribution. In conclusion, cloud clearing increases global coverage significantly, making daily monitoring possible, without causing large biases in the tropospheric CO retrievals.

ACPD
13, 16337–16366, 2013

4 Distinguishing CO emissions from the background using AIRS measurements

Emission inventories based on direct CO measurements have not been available except with the use of inverse modeling techniques. This study attempts to draw information on new emissions from CO data directly to benefit the ultimate goal of monitoring fire activities in near-real time. As shown in Fig. 6, the CO variation for the background (blue curves) and emissions (red curves) can be analyzed separately. We use the clear sky only cases in the following sections because the CO variability for both the background values and the new emissions are better defined (see Fig. 6) and agree better with our previous knowledge of the CO distribution.

To quantify the quality of the emission data from AIRS CO, we compare them with existing biomass burning and anthropogenic emission inventories. The version 3 of the Global Fire Emissions Database (GFED3) biomass burning inventory (Van der Werf et al., 2010) used a revised version of the Carnegie–Ames–Stanford–Approach (CASA) biogeochemical model and improved satellite-derived estimates of area burned, fire activity, and plant productivity to calculate fire emissions for the 1997–2009 period on a $0.5^{\circ} \times 0.5^{\circ}$ spatial resolution with a monthly time step. For November 2000 onwards, estimates were based on burned area, active fire detections, and plant productivity from the MODIS sensor. For anthropogenic emissions without counting biomass burnings, we use the data that were produced as part of MACC/CityZEN UE (MACCity) project and are available on the Ether/ECCAD-GEIA database. The dataset MACCity is part of the Atmospheric Chemistry and Climate – Model Inter comparison Project (ACCMIP), and focuses on the anthropogenic emission from 1960 to 2010 with a spatial resolution of $0.5^{\circ} \times 0.5$.

Figure 7 shows the variability of AIRS CO new emission (red dotted curves) and that of other inventory data (green dotted curves), i.e., the total amount of GFED3 biomass burning and MACCity anthropogenic without biomass burning emissions, for the NH (upper panel) and the SH (lower panel), respectively. We have also filtered AIRS CO

ACPD
13, 16337–16366, 2013

new emissions (red solid curve), and the inventories (green solid curve), using Butterworth lowpass filter in the third order with a Fast Fourier Transform. The seasonal and inter-annual cycles agree very well in the time domain although the relative magnitudes are different. Note also the units between the two datasets are different. In the NH, the maximum peaks in late winter and early spring, while in certain years (2006, 2007, 2008, and 2010) there is a secondary maximum in the summer likely due to biomass burning events. There is also a noticeable lag in the AIRS new emission in the NH compared to the inventories from 2006 to 2009, possibly due to the fact the smoothed peaks in AIRS incorporated the summer burning events in these years. In the SH, both CO variability phase and relative magnitudes agree very well between AIRS CO emissions and the inventories.

The correlations are computed between AIRS CO VMRs emissions and the total emission amount of GFED3 and MACCity inventories for the NH and SH as shown in Fig. 8 left panel and right panel, respectively. The correlation coefficients are 0.726 for the NH and 0.915 for the SH. The higher correlation coefficient in the SH land cases is due to the fact that most of the emissions are from large and persistent fires, which are easier to detect by satellite sensors. In the NH, the non-biomass burning anthropogenic emissions are more difficult to quantify since the sensitivity of the thermal sensors in the boundary layer is low where the pollution emission is high.

5 Continued CO variability with IASI measurements

As the first step to quantify the uncertainties of the CO measurements from AIRS and IASI, we examine the differences between these two operational CO products. These two products are based on a similar retrieval algorithm (the AIRS physical retrieval algorithm), as described by Susskind et al. (2003), but cross-calibration has not been sufficient to establish consistent climate data records. The advantage of this algorithm is that it provides accurate retrievals where the measurement signals are strong, and the major disadvantages lie where the measurement signals are weak (Warner et al.,

ACPD
13, 16337–16366, 2013

2007, 2010), in which case the information is dominated by the a priori or first guess. The main difference between AIRS and IASI in the CO region is reflected through the spectral resolution. Figure 9 shows a comparison of the two spectra with AIRS CO region in the upper panel and IASI in the lower panel. AIRS bands only cover the CO R-branch and have a much lower spectral resolution than IASI, but higher Signal-to-Noise Ratio (SNR) (George et al., 2009). Nonetheless, AIRS CO obtains highly accurate retrievals in the mid-troposphere despite the relatively lower spectral resolution and a narrower CO band, as shown in previous validation studies (Warner et al., 2007; McMillan et al., 2010).

Similar to the fact that AIRS uses 9 FOVs per FOR to match AMSU footprints for cloud clearing, IASI uses 4 FOVs per FOR to match Advanced Very High Resolution Radiometer (AVHRR) (Frey et al., 2012) footprints. We use IASI L2 cloud information to identify clear scenes for this study rather than using additional cloud screening from AVHRR as discussed for the case of AIRS using the MODIS cloud mask. This will create some uncertainties to the CO variability study, however, we do not expect large differences as can be seen in Fig. 2 upper versus lower panels for the case of AIRS.

Figure 10 shows an example of the direct inter-comparison of CO VMRs at 500 hPa averaged over four seasons for the years 2002–2011 (December–February in a; March–May in b; June–August in c; and September–November in d) between AIRS (top panel), IASI (middle panel), and the differences (AIRS-IASI) (bottom panel), respectively. The differences in the bottom panels show approximately less than ±15 ppbv between AIRS and IASI except over several problematic regions for the retrievals, i.e. Antarctica, Greenland, the South America coast near Chile, and over the Southern Ocean. In general, AIRS CO is higher than IASI in the NH by less than 10 ppbv or 10 % and slightly higher over elevated CO regions. This is particularly true in the NH winter season (December) through late spring (May). The differences between AIRS and IASI CO in the NH are mainly due to the magnitude and location of the CO plumes, which is partly due to the local time difference between AIRS (09:30 LT) and IASI (13:30 LT) measurements. IASI CO values are higher than AIRS over the biomass burning plumes

ACPD
13, 16337–16366, 2013

in the tropics and lower elsewhere. In the SH, AIRS CO at 500 hPa is higher than IASI CO by 15–20 ppbv, which is a known bias from AIRS CO due to the use of one global a priori or first guess (Warner et al., 2010). The more accurate IASI CO in the SH is most likely due to the increased information content in the vertical range by having a larger number of spectral bands and high spectral resolution (see Fig. 9). Persistent biases between the two datasets over Antarctica, Greenland, and Chile are largely due to IASI CO being too low. This is likely due to cold surfaces at IASI's morning overpass local time providing reduced measurement sensitivity. Seasonally, the CO values are highest in March–May in the NH due to higher emissions and slower CO removal process with lower OH concentrations. In the months of September–November, strong biomass burning events occur in the SH emitting high amounts of CO.

We take a similar approach as described in the previous sections to discuss the CO variability and short-term trends of IASI with an emphasis on consistency tests with AIRS. We again begin with the normalized monthly CO PDFs of IASI under clear sky conditions and fit two Gaussian functions to each monthly PDF. The modes are treated as biases from the Gaussian fits to show the CO variability from September 2008 to December 2012 as shown in Fig. 11. AIRS background CO is plotted in blue, emissions in red, and the IASI background is in cyan, and emissions in orange. AIRS and IASI agree very well over land where the measurement sensitivities are higher in general due to the higher surface thermal contrast (Deeter et al., 2007); while IASI CO is lower than AIRS over ocean for the emission and background CO in both NH and SH. For both AIRS and IASI, the new emissions are higher than background CO values and more variable.

We used linear fits to the CO variability from the modes of the Gaussian PDFs for background values and the new emission separately; and the rates are listed in Table 1. We find the AIRS CO short-term trends in the NH are decreasing from 2002 to the mid of 2011 at a rate of $-1.71\,\mathrm{ppbv\,yr^{-1}}$ at 500 hPa for both new emissions and the background CO. Over the NH Ocean the transported new emissions decrease faster than the background CO at 500 hPa at a rate of $-1.95\,\mathrm{ppbv\,yr^{-1}}$ and $-1.18\,\mathrm{ppbv\,yr^{-1}}$, re-

ACPD
13, 16337–16366, 2013

spectively. The background CO over the ocean decreases at a slower rate than the new emissions; and this may be due to the lack of mixing compared to over land. The CO decreasing rates are lower in the SH than in the NH, with the new emissions decreasing at a rate of $-0.14\,\mathrm{ppbv\,yr^{-1}}$ and background CO decreasing at $-0.28\,\mathrm{ppbv\,yr^{-1}}$, respectively, at 500 hPa over land. Over the SH ocean the CO decreasing trends are similar for the transported new emissions ($-0.85\,\mathrm{ppbv\,yr^{-1}}$) and the background values ($-0.62\,\mathrm{ppbv\,yr^{-1}}$). The fact that the emission reduction in the NH is larger compared to the SH indicates that the primary cause of the emission reduction is the change in pollution sources due to regulations, and is also likely associated with economic slowdown in the last decade.

IASI CO, however, shows a noticeable increase from the beginning of 2009 to the end of 2012 except for over the SH ocean where the linear fits decrease by small amounts of -0.63 and $-0.35\,\mathrm{ppbv\,yr^{-1}}$ for the transported new emissions and the background CO, respectively. The CO increases over NH land and ocean and SH land, range from 2.26 to 3.23 $\mathrm{ppbv\,yr^{-1}}$ for the background values and from 4.45 to 5.14 $\mathrm{ppbv\,yr^{-1}}$ for the new emissions. Although the data record for this time frame is too short for this result to be conclusive, the CO values are higher in 2012 compared to the CO values in 2009.

6 Summary

The goal of this study is to understand the global CO variability and short-term trends for the background values and new emissions separately. We use an innovative approach to statistically separate the new emissions from the background CO in the satellite datasets by using PDF analyses. We have demonstrated that this technique works well by showing good correlation between the AIRS CO emissions we obtained and the established inventory database (i.e., GFED3 and MACCity) with correlation coefficients of 0.726 in the NH and 0.915 in the SH, respectively.

To ensure that we use the highest quality data for this study, we examine a potential error source due to the treatment of clouds in AIRS retrieval algorithm. We first iden-

ACPD
13, 16337–16366, 2013

tified AIRS clear sky single FOV pixels by using collocated MODIS cloud masks such that in each AIRS pixel 99 % of MODIS pixels are flagged as being clear. We found that, overall, there is little difference in the location of the elevated CO plumes between the clear sky cases and the cloud cleared retrievals. Under clear sky conditions, however, we showed the DOFS are higher than for the cloud-cleared cases. Although the CO values do not exhibit biases between the clear sky and cloud-cleared conditions when statistically averaged for the NH land, NH ocean, SH land, and SH ocean, the CO variability for clear sky cases is better defined. Therefore, we used clear sky only cases for the variability and short-term trend studies in Sects. 4 and 5.

Climate and trend studies rely on continued and unbiased long-term data records. For tropospheric CO, it is ideal to used AIRS and IASI jointly with cross-validated datasets. This study carried out a thorough comparison between AIRS and IASI CO operational products in terms of their distribution and variability. We focused on the short-term trends of the joint CO distribution from AIRS and IASI, and separately for the new emissions and the background CO. We found that the global AIRS CO at 500 hPa has shown a decreasing trend from 2003 through 2010 with a larger reduction in the NH than in the SH. IASI CO, which is more indicative of the data short-term trend from 2009 through 2012, shows an increased distribution over the NH land and ocean, and the SH land. This study will be extended with the current AIRS and IASI and future sensors.

Acknowledgements. This study is supported by the NASA Earth Sciences through ROSES by: the Climate Record Uncertainty Analysis Program (NNX11AL22A), and by the sub-contract by NASA JPL AIRS team (2009–2010). We have also been partially supported by RTRA/STAE foundation from Toulouse, France. The authors wish to thanks AIRS, IASI, and MODIS science teams and Ether for the wonderful products that made these measurements possible.

ACPD
13, 16337–16366, 2013

References

Ackerman, S. A., Strabala, K. I., Menzel, W. P., Frey, R. A., Moeller, C. C., and Gumley, L. E.: Discriminating clear sky from clouds with MODIS, J. Geophys. Res., 103, 32141–32157, 1998.

Arellano, A. F. and Hess, P.: Sensitivity of top-down estimates of CO sources to GCTM transport, Geophys. Res. Lett., 33, L21807, doi:10.1029/2006GL027371, 2006.

Arellano Jr., A. F., Raeder, K., Anderson, J. L., Hess, P. G., Emmons, L. K., Edwards, D. P., Pfister, G. G., Campos, T. L., and Sachse, G. W.: Evaluating model performance of an ensemble-based chemical data assimilation system during INTEX-B field mission, Atmos. Chem. Phys., 7, 5695–5710, doi:10.5194/acp-7-5695-2007, 2007.

Aumann, H. H., Chahine, M. T., Gautier, C., Goldberg, M., Kalnay, E., McMillin, L., Revercomb, H., Rosenkranz, P. W., Smith, W. L., Staelin, D., Strow, L., and Susskind, J.: AIRS/AMSU/HSB on the Aqua mission: design, science objectives, data products and processing systems, IEEE T. Geosci. Remote, 41, 253–264, 2003.

Beer, R.: TES on the Aura mission: scientific objectives, measurements, and analysis overview, IEEE T. Geosci. Remote, 44, 1102–1105, 2006.

Chahine, M. T.: Remote sounding cloudy atmospheres, I. The single cloud layer, J. Atmos. Sci., 31, 233–243, 1974.

Chahine, M. T.: Remote sounding cloudy atmospheres, II. Multiple cloud formations, J. Atmos. Sci., 34, 744–757, 1977.

Chevalier, A., Gheusi, F., Attié, J.-L., Delmas, R., Zbinden, R., Athier, G., and Cousin, J.-M.: Carbon monoxide observations from ground stations in France and Europe and long trends in the free troposphere, Atmos. Chem. Phys. Discuss., 8, 3313–3356, doi:10.5194/acpd-8-3313-2008, 2008.

Clerbaux, C., Turquety, S., and Coheur, P. F.: Infrared remote sensing of atmospheric composition and air quality: towards operational applications, C. R. Geosci., 342, 349–356, doi:10.1016/j.crte.2009.09.010, 2010.

Deeter, M. N., Edwards, D. P., Gille, J. C., and Drummond, J. R.: Sensitivity of MOPITT observations to carbon monoxide in the lower troposphere, J. Geophys. Res., 112, D24306, doi:10.1029/2007JD008929, 2007.

Drummond, J. R.: Novel correlation radiometer: the length modulated radiometer, Appl. Optics, 28, 2451–2452, 1989

ACPD
13, 16337–16366, 2013

Emmons, L. K., Deeter, M. N., Gille, J. C., Edwards, D. P., Attié, J.-L., Warner, J., Ziskin, D., Francis, G., Khattatov, B., Yudin, V., Lamarque, J.-F., Ho, S.-P., Mao, D., Chen, J. S., Drummond, J., Novelli, P., Sachse, G., Coffey, M. T., Hannigan, J. W., Gerbig, C., Kawakami, S., Kondo, Y., Takegawa, N., Schlager, H., Baehr, J., and Ziereis, H.: Validation of Measurements of Pollution in the Troposphere (MOPITT) CO retrievals with aircraft in situ profiles, J. Geophys. Res., 109, D03309, doi:10.1029/2003JD004101, 2004.

Emmons, L. K., Pfister, G. G., Edwards, D. P., Gille, J. C., Sachse, G., Blake, D., Wofsy, S., Gerbig, C., Matross, D., and Neìdeìlec, P.: Measurements of Pollution in the Troposphere (MOPITT) validation exercises during summer 2004 field campaigns over North America, J. Geophys. Res., 112, D12S02, doi:10.1029/2006JD007833, 2007.

Fisher, J. A., Jacob, D. J., Purdy, M. T., Kopacz, M., Le Sager, P., Carouge, C., Holmes, C. D., Yantosca, R. M., Batchelor, R. L., Strong, K., Diskin, G. S., Fuelberg, H. E., Holloway, J. S., Hyer, E. J., McMillan, W. W., Warner, J., Streets, D. G., Zhang, Q., Wang, Y., and Wu, S.: Source attribution and interannual variability of Arctic pollution in spring constrained by aircraft (ARCTAS, ARCPAC) and satellite (AIRS) observations of carbon monoxide, Atmos. Chem. Phys., 10, 977–996, doi:10.5194/acp-10-977-2010, 2010.

Frey, C., Kuenzer, C., and Dech, S.: Quantitative comparison of the operational NOAA AVHRR LST product of DLR and the MODIS LST product V005, Int. J. Remote Sens., 33, 7165–7183, doi:10.1080/01431161.2012.699693, 2012.

George, M., Clerbaux, C., Hurtmans, D., Turquety, S., Coheur, P.-F., Pommier, M., Hadji-Lazaro, J., Edwards, D. P., Worden, H., Luo, M., Rinsland, C., and McMillan, W.: Carbon monoxide distributions from the IASI/METOP mission: evaluation with other space-borne remote sensors, Atmos. Chem. Phys., 9, 8317–8330, doi:10.5194/acp-9-8317-2009, 2009.

He, H., Stehr, J. W., Hains, J. C., Krask, D. J., Doddridge, B. G., Vinnikov, K. Y., Canty, T. P., Hosley, K. M., Salawitch, R. J., Worden, H. M., and Dickerson, R. R.: Trends in emissions and concentrations of air pollutants in the lower troposphere in the Baltimore/Washington airshed from 1997 to 2011, Atmos. Chem. Phys. Discuss., 13, 3135–3178, doi:10.5194/acpd-13-3135-2013, 2013.

Justice, C. O., Giglio, L., Korantzi, S., Owens, J., Morisette, J., Roy, D., Dcscloitres, J., Alleaume, S., Petitcolin, F., and Kaufman, Y.: The MODIS fire products, Remote Sens. Environ., 83, 244–262, 2002.

ACPD
13, 16337–16366, 2013

Kim, P. S., Jacob, D. J., Liu, X., Warner, J. X., Yang, K., and Chance, K.: Global ozone–CO correlations from OMI and AIRS: constraints on tropospheric ozone sources, Atmos. Chem. Phys. Discuss., 13, 8901–8937, doi:10.5194/acpd-13-8901-2013, 2013.

Kopacz, M., Jacob, D. J., Fisher, J. A., Logan, J. A., Zhang, L., Megretskaia, I. A., Yantosca, R. M., Singh, K., Henze, D. K., Burrows, J. P., Buchwitz, M., Khlystova, I., McMillan, W. W., Gille, J. C., Edwards, D. P., Eldering, A., Thouret, V., and Nedelec, P.: Global estimates of CO sources with high resolution by adjoint inversion of multiple satellite datasets (MOPITT, AIRS, SCIAMACHY, TES), Atmos. Chem. Phys., 10, 855–876, doi:10.5194/acp-10-855-2010, 2010.

Lamarque, J.-F., Khattatov, B., Yudin, V., Edwards, D. P., Gille, J. C., Emmons, L. K., Deeter, M. N., Warner, J., Ziskin, D., Francis, G., Ho, S., Mao, D., and Chen, J.: Application of a bias estimator for the improved assimilation of Measurements of Pollution in the Troposphere (MOPITT) carbon monoxide retrievals, J. Geophys. Res., 109, D16304, doi:10.1029/2003JD004466, 2004.

Lin, M., Fiore, A., Horowitz, L. W., Cooper, O. R. R., Naik, V., Holloway, J. S., Johnson, B. J. J., Middlebrook, A. M., Oltmans, S. J. J., Pollack, I. B., Ryerson, T. B., Warner, J., Wiedinmyer, C., Wilson, J., and Wyman, B.: Transport of Asian ozone pollution into surface air over the western United States in spring, J. Geophys. Res., 117, D00V07, doi:10.1029/2011JD016961, 2011.

McMillan, W. W., Evans, K. D., Barnet, C. D., Maddy, E. S., Sachse, G. W., and Diskin, G. S.: AIRS V5 CO retrieval with DACOM in situ measurements, IEEE T. Geosci. Remote, 49, 7, 2011.

McMillin, L. M. and Dean, C.: Evaluation of a new operational technique for producing clear radiances, J. Appl. Meteor., 21, 1005–1014, 1982.

Pfister, G., Hess, P. G., Emmons, L. K., Lamarque, J.-F., Wiedinmyer, C., Edwards, D. P., Petron, G., Gille, J. C., and Sachse, G. W.: Constraints on emissions for the Alaskan wildfires 2004 using data assimilation and inverse modeling of MOPITT CO, 2005, Geophys. Res. Lett., 32, L11809, doi:10.1029/2005GL022995, 2005.

Pradier, S., Attie, J.-L., Chong, M., Escobar, J., Peuch, V.-H., and Lamarque, J.-F., Khattatov, B., and Edwards, D. P.: Evaluation of 2001 springtime CO transport over West Africa using MOPITT CO measurements assimilated in a global chemistry transport model, Tellus B, 58, 163–176, 2006.

ACPD
13, 16337–16366, 2013

Smith, W. L.: An improved method for calculating tropospheric temperature and moisture from satellite radiometer measurements, Mon. Weather Rev., 96, 387–396, 1968.
Susskind, J., Barnet, C., and Blaisdell, J.: Determination of atmospheric and surface parameters from simulated AIRS/AMSU/HSB sounding data: retrieval and cloud clearing methodology, Adv. Space Res., 21, 3, 1998, 369–384, 1998.
Susskind, J., Barnet, C. D., and Blaisdell, J. M.: Retrieval of atmospheric and surface parameters from AIRS/AMSU/HSB data in the presence of clouds, IEEE T. Geosci. Remote, 41, 390–409, 2003.
van der Werf, G. R., Randerson, J. T., Giglio, L., Collatz, G. J., Mu, M., Kasibhatla, P. S., Morton, D. C., DeFries, R. S., Jin, Y., and van Leeuwen, T. T.: Global fire emissions and the contribution of deforestation, savanna, forest, agricultural, and peat fires (1997–2009), Atmos. Chem. Phys., 10, 11707–11735, doi:10.5194/acp-10-11707-2010, 2010.
Warner, J. X., Gille, J. C., Edwards, D. P., Ziskin, D. C., Smith, M. W., and Bailey, P. L.: Cloud detection and clearing for the EOS Terra satellite Measurement of Pollution in the Troposphere (MOPITT) experiment, Appl. Optics, 40, 1269–1284, 2001.
Warner, J. X., Comer, M. M., Barnet, C. D., McMillan, W. W., Wolf, W., Maddy, E., and Sachse, G.: A comparison of satellite tropospheric carbon monoxide measurements from AIRS and MOPITT during INTEX-A, J. Geophys. Res., 112, D12S17, doi:10.1029/2006JD007925, 2007.
Warner, J. X., Wei, Z., Strow, L. L., Barnet, C. D., Sparling, L. C., Diskin, G., and Sachse, G.: Improved agreement of AIRS tropospheric carbon monoxide products with other EOS sensors using optimal estimation retrievals, Atmos. Chem. Phys., 10, 9521–9533, doi:10.5194/acp-10-9521-2010, 2010.
Worden, H. M., Deeter, M. N., Frankenberg, C., George, M., Nichitiu, F., Worden, J., Aben, I., Bowman, K. W., Clerbaux, C., Coheur, P. F., de Laat, A. T. J., Detweiler, R., Drummond, J. R., Edwards, D. P., Gille, J. C., Hurtmans, D., Luo, M., Martínez-Alonso, S., Massie, S., Pfister, G., and Warner, J. X.: Decadal record of satellite carbon monoxide observations, Atmos. Chem. Phys., 13, 837–850, doi:10.5194/acp-13-837-2013, 2013.

ACPD
13, 16337–16366, 2013

Table 1. The rates of the reduction/increase of CO VMRs at 500 hPa for the background values and the new emissions from AIRS and IASI.

	AIRS CO VMRs at 500 hPa 2003–2011		IASI CO VMRs at 500 hPa 2009–2012	
	Emissions	Background	Emissions	Background
NH Land	−1.71	−1.71	4.49	2.26
NH Ocean	−1.95	−1.18	4.45	3.23
SH Land	−0.14	−0.28	5.14	2.77
SH Ocean	−0.85	−0.62	−0.63	−0.35

ACPD
13, 16337–16366, 2013

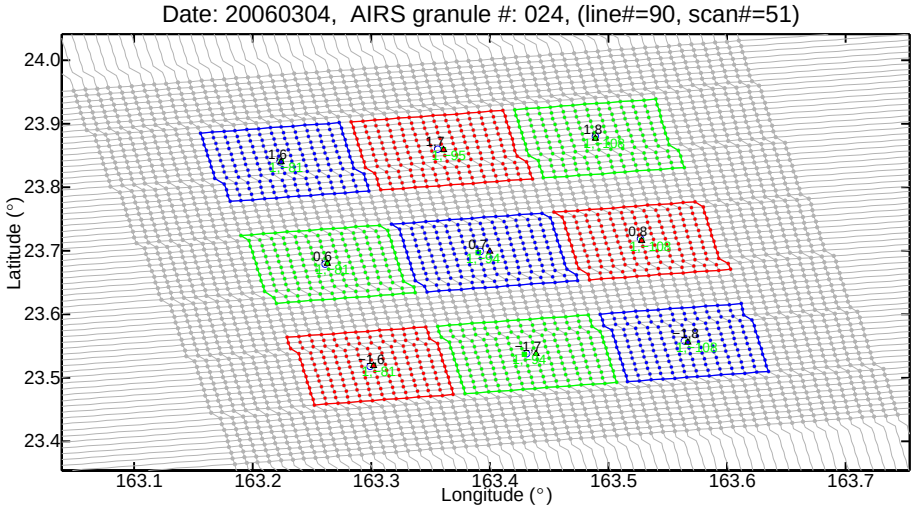

Fig. 1. An example to illustrate the collocation method between AIRS and MODIS pixels.

ACPD
13, 16337–16366, 2013

Tropospheric carbon monoxide variability from AIRS and IASI

J. Warner et al.

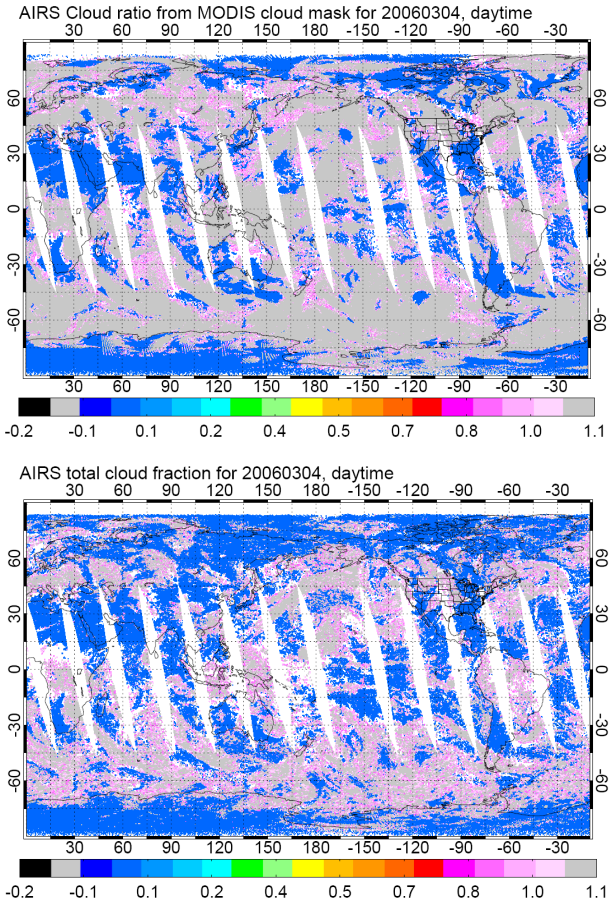

Fig. 2. AIRS cloud coverage defined by the MODIS cloud mask (upper panel) and defined by AIRS L2 products where CloudFraction = 0 (lower panel).

ACPD
13, 16337–16366, 2013

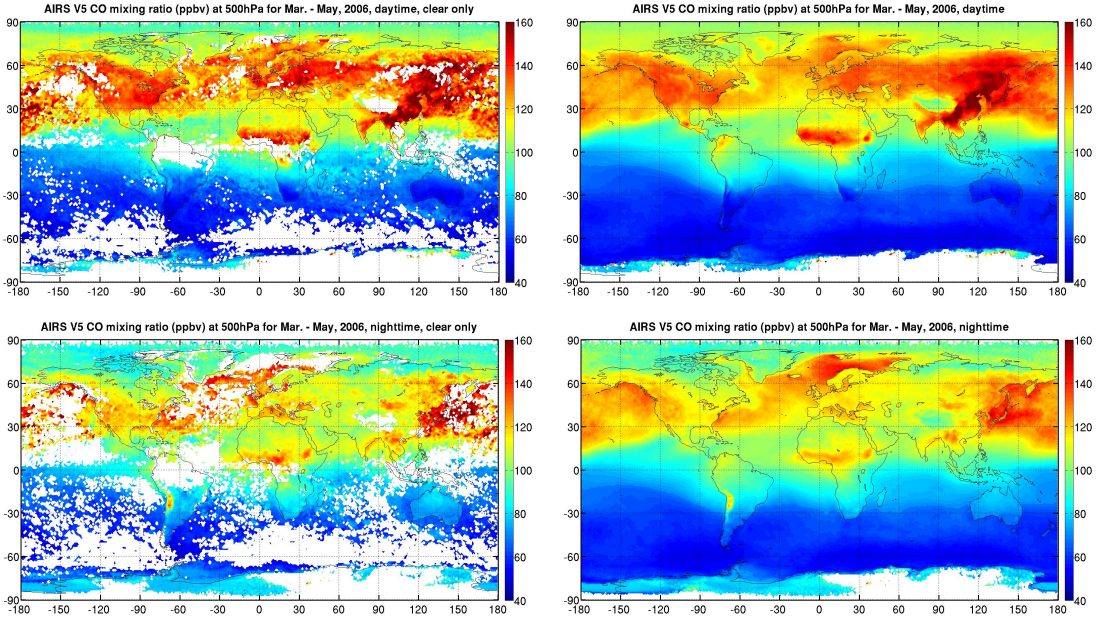

Fig. 3. The three-months mean AIRS V5 CO maps for March to May 2006 with the clear sky daytime cases (left upper panel), the clear sky nighttime cases (left bottom panel), the cloud-cleared daytime cases (right upper panel), and the cloud-cleared nighttime cases (right bottom panel).

ACPD
13, 16337–16366, 2013

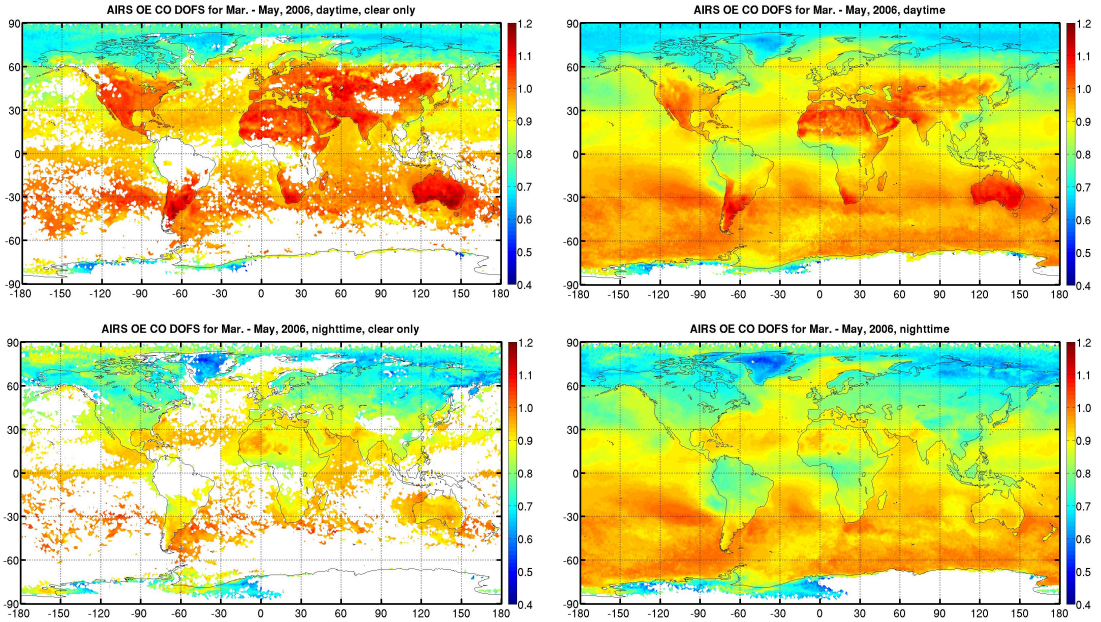

Fig. 4. AIRS OE CO DOFS for the months of March to May 2006 for cloud-cleared cases (right panels) versus clear cases (left panels) and for daytime (upper panels) versus nighttime (lower panels).

ACPD
13, 16337–16366, 2013

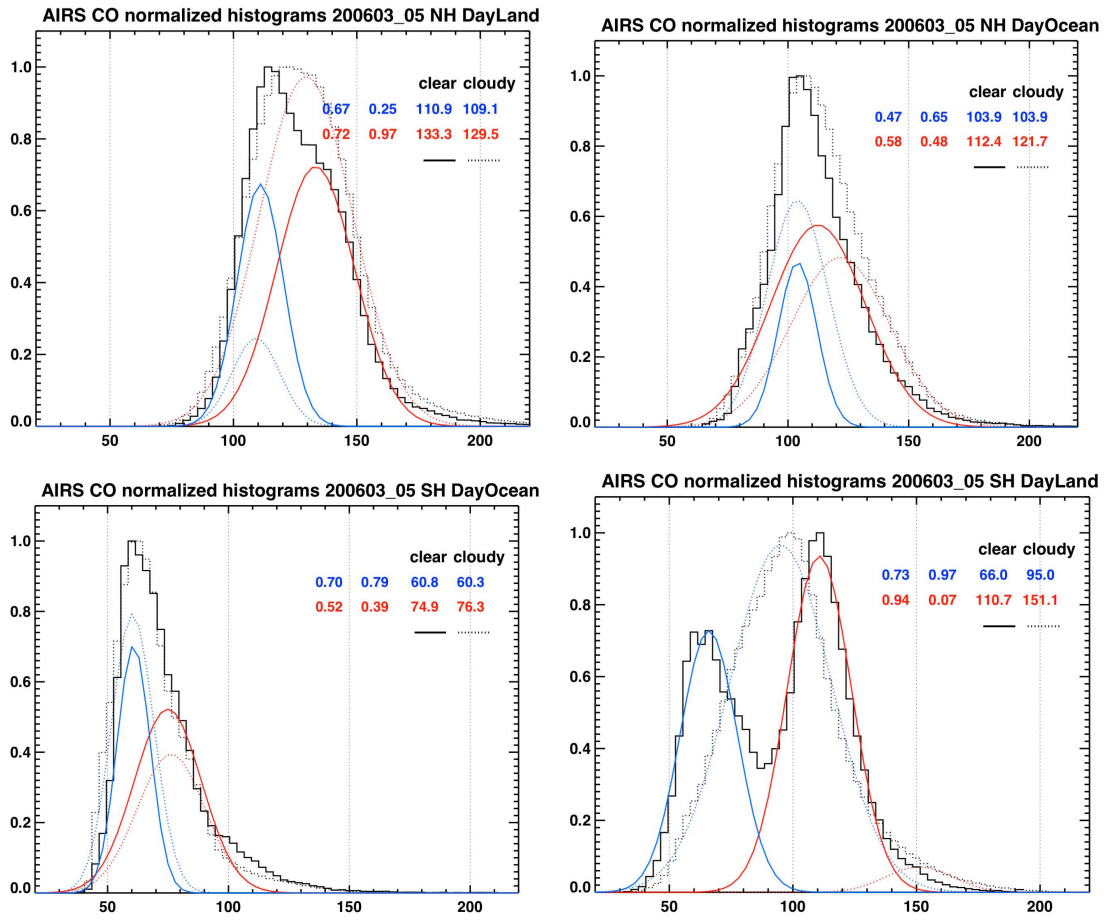

Fig. 5. The monthly mean CO VMRs for March to May 2006 using PDFs for the NH ocean (upper left), NH land (upper right), SH ocean (lower left), and SH land (lower right), respectively, for daytime only.

ACPD
13, 16337–16366, 2013

Tropospheric carbon monoxide variability from AIRS and IASI

J. Warner et al.

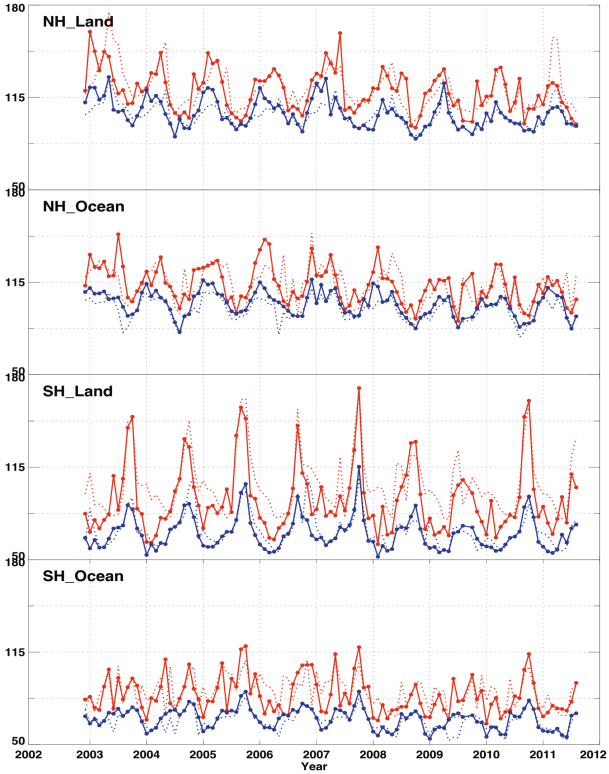

Fig. 6. Tropospheric CO variability from 2002 through 2011, which uses the modes of the fitted Gaussian functions for each monthly PDF to represent biases, for emissions (red curves) and the background (blue curves), for clear sky cases (solid) and cloud-cleared (dotted), and for NH-Land (top panel), NH-Ocean (2nd panel), SH-Land (3rd panel), and SH-Ocean (bottom panel), respectively.

ACPD
13, 16337–16366, 2013

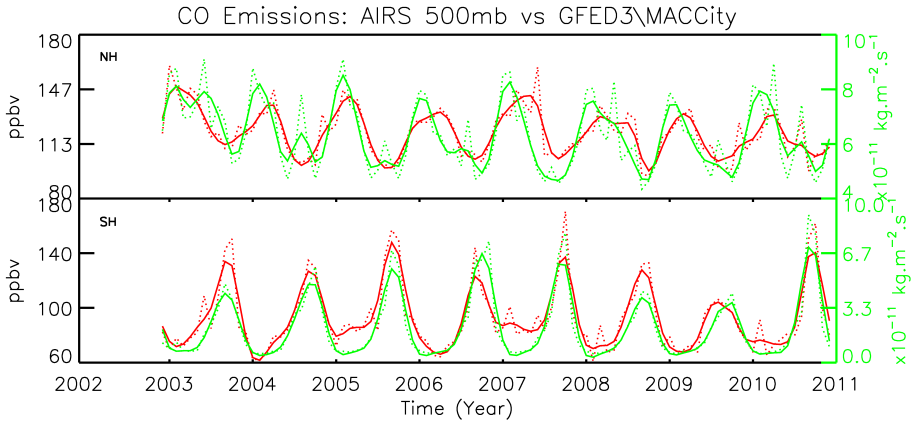

Fig. 7. The variability of AIRS CO new emission (red dotted curves) and that of other inventory data (green dotted curves), i.e., the total amount of GFED3 biomass burning and MACCity anthropogenic without biomass burning emissions, for the NH (upper panel) and the SH (lower panel), respectively. The smoothed AIRS CO new emissions using a second-degree polynomial function (red solid curve), and smoothed the inventories (green solid curve) are also shown.

ACPD
13, 16337–16366, 2013

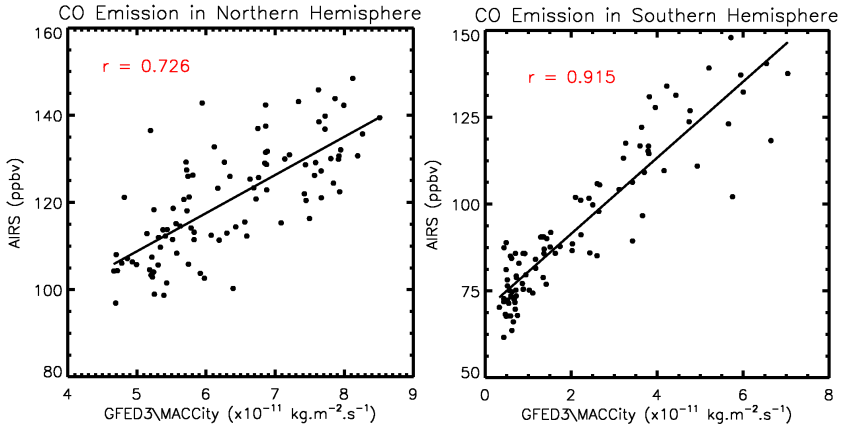

Fig. 8. The correlations between AIRS CO VMR emissions and the total emission amount of GFED3 and MACCity inventories for the NH (left panel) and SH (right panel), respectively.

ACPD
13, 16337–16366, 2013

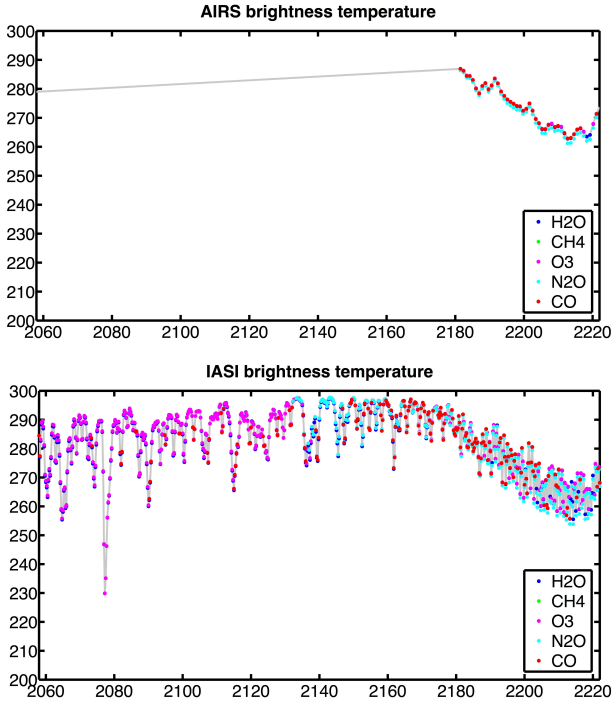

Fig. 9. Brightness temperatures for AIRS' (top) and IASI's (bottom) spectrum with major atmospheric constituents.

ACPD
13, 16337–16366, 2013

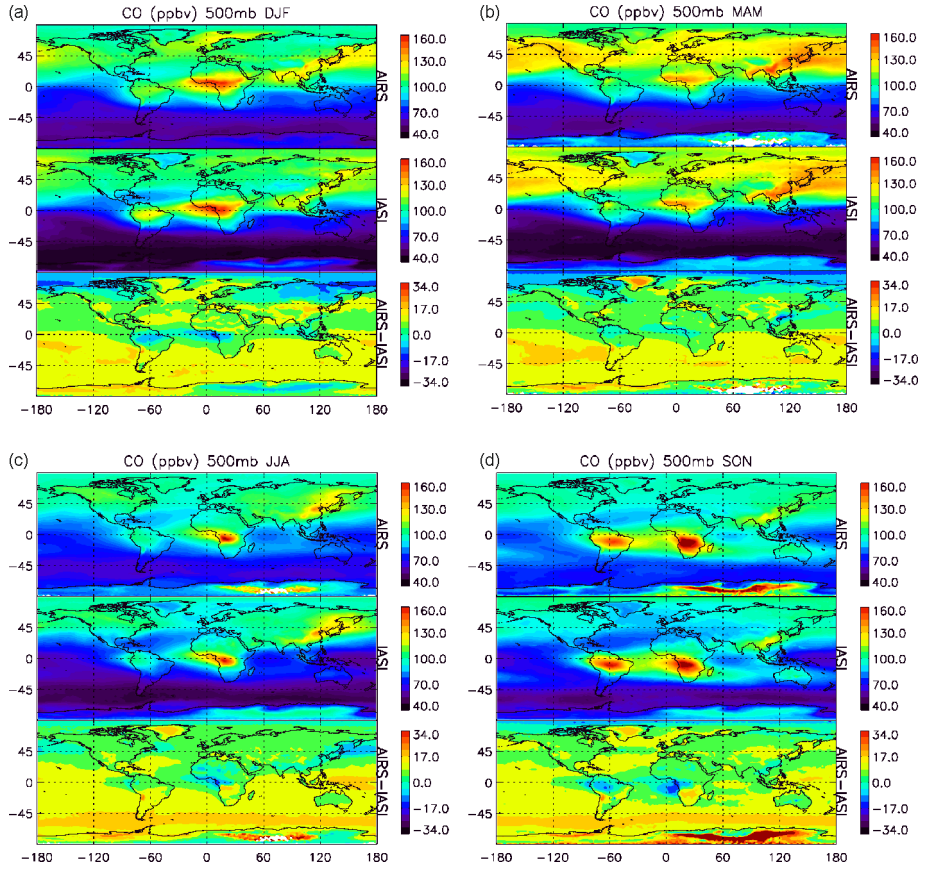

Fig. 10. An example of the direct inter-comparison of CO VMRs at 500 hPa averaged over four seasons for the years 2002–2011 (December–February in **(a)**; March–May in **(b)**; June–August in **(c)**; and September–November in **(d)** between AIRS (top panel), IASI (middle panel), and the differences (AIRS-IASI) (bottom panel), respectively.

ACPD
13, 16337–16366, 2013

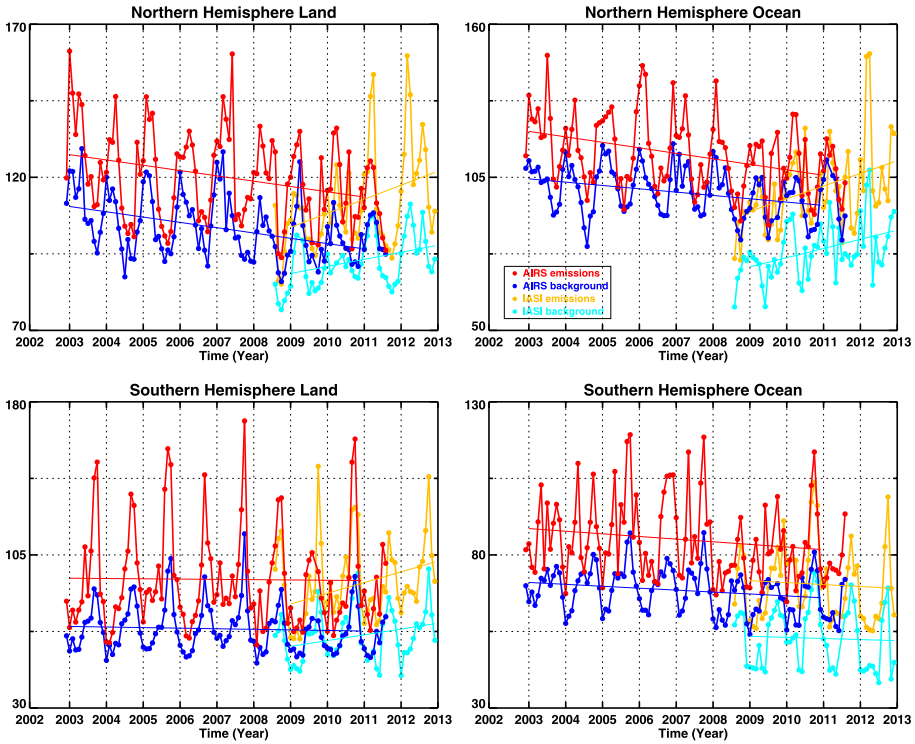

Fig. 11. Similarly to Fig. 6, except for AIRS clear sky only cases from 2002 to 2011 and for IASI clear sky CO variability from September 2008 to December 2012.

ACPD
13, 16337–16366, 2013

Tropospheric carbon monoxide variability from AIRS and IASI

J. Warner et al.